Polyoxometalate complexes as precursors to vanadium doped-molybdenum or tungsten oxide thin films *via* aerosol-assisted CVD

Sapna Ponja, Sanjayan Sathasivam[a,b], Hywel O. Davies[c], Ivan P. Parkin[a] and Claire J. Carmalt[a]*

*Corresponding author

[a]Materials Chemistry Centre, Department of Chemistry, University College London, 20 Gordon Street, London WC1H 0AJ, UK

Fax: (+44) 20-7679-7463

E-mail: c.j.carmalt@ucl.ac.uk

[b]Bio Nano Consulting Ltd, The Gridiron Building, One St. Pancras Square, London N1C 4AG, UK

Fax: (+44) 20-7396-1056

E-mail: info@bio-nano-consulting.com

[c]ACAL Energy Ltd, Heath Business and Technology Park, Runcorn WA7 4QX, Cheshire, England.

Abstract

Aerosol assisted chemical vapour deposition of substituted polyoxometalates: $H_4[PMo_{11}VO_{40}]$; $H_7[PMo_8V_4O_{40}]$; $[^nBu_4N]_4[PVW_{11}O_{40}]$ and $[^nBu_4N]_5[PV_2W_{10}O_{40}]$ resulted in the formation of vanadium-doped metal oxide thin films. Depositions were carried out at 550 ^oC in methanol or acetonitrile solution for the molybdenum or tungsten containing POMs, respectively. The as-deposited films were X-ray amorphous and relatively non-adherent however, on annealing in air at 600 ^oC decolourised translucent films which were more mechanically robust were obtained. Films deposited from $H_4[PMo_{11}VO_{40}]$ and $H_7[PMo_8V_4O_{40}]$ consisted of V-doped MoO_3 in the orthorhombic phase and films from $[^nBu_4N]_4[PVW_{11}O_{40}]$ and $[^nBu_4N]_5[PV_2W_{10}O_{40}]$ comprised of monoclinic V-doped WO_3. All films were fully characterised using XPS, EDX, SEM and UV-Vis.

Introduction

Polyoxometalates (POMs) are characterized as anionic transition metal oxygen cluster compounds, diverse in structure,[1] physical and chemical properties, that lend themselves to a wide range of applications, most notably as catalysts and conductive materials, in the form of membranes and thin films.[2] POM clusters have a high degree of solubility in a variety of inorganic and organic solvents and hence are termed 'molecular metal oxides'.[2a] In solution, POMs interact electrostatically with cationic species which leads to interactions between POMs and cationic ions, molecules, complexes, polymers and positively charged solid surfaces.[2a] POMs are classified into two subfamilies depending on the absence (as in heteropolyanions) or presence (as in isopolyanions) of a central cation or heteroatom.[1] A number of different structural types of POM clusters exist[1, 2b] but the Keggin structure was the first to be discovered.[1] Keggin-type POMs can be represented by the formula $[XM_{12}O_{40}]^{n-}$ where X is the central heteroatom (e.g., P, Si, or B) with 4 oxygen atoms bonded tetrahedrally to it, and M (usually Mo, W or V) is the addenda or peripheral atom (the metal atoms that make up the framework). The central atom is surrounded by 12 octahedrons made of MO_6 and all the oxygens are shared except for the 12 terminal oxygens, which are attached to only one atom.

Substituted POMs are a modification of the Keggin structure where an additional addenda atom can be incorporated, such as vanadium to give POMs of formula, $[PM_{12-x}V_xO_{40}]^{n-}$.[3] The physical and chemical properties of a POM are a function of their chemical composition, i.e. the identity of the heteroatom and addenda atom(s). POMs with Mo or W as the addenda atoms with different heteroatoms (e.g., P, V, Nb or W) are easy to prepare. Changing the heteroatom and/or substituting an addenda atom also provides the means to add an additional element into the metal oxide films which may have a significant effect on the chemical and physical properties of the film and lead to doped-metal oxide films. Vanadium has been used as a dopant in the production of thin films for reducing the band gap and improving photocatalytic properties.[4]

Thin films of Mo oxides have been made previously using dual-source precursors, such as molybdenum hexacarbonyl, $[Mo(CO)_6]$ and oxygen, and from single-source precursors such as molybdenum pentacarbonyl 1-methylbutylisonitrile.[5]

Molybdenum(VI) oxide exists in two basic crystal structures with different molecular vibrational and optical properties:[5] α-MoO_3 with orthorhombic symmetry and metastable monoclinic β-MoO_3; MoO_2 also has a monoclinic structure.[6] Molybdenum trioxide (MoO_3), the technologically more significant form of the oxide, exists in the orthorhombic phase and has a double layered structure.[6] MoO_3 is a well-known catalyst often used in the oxidative dehydrogenation of methanol to an aldehyde[7] and has also been shown to act as an excellent antimicrobial coating, forming an acidic environment that retards bacterial growth and proliferation.[8] Applications of MoO_3 also extend to organic electronic devices due to its low absorption in the visible spectrum and high compatibility with other materials. MoO_3 has also been used as a material to reduce energy barriers for charge carrier injection, extraction or transport between semiconductor and organic layers.[9]

Like MoO_3, tungsten trioxide (WO_3) has many applications as an interface layer in electronic devices.[9-10] Principally, it reduces the barrier for charge injection between, for example, a tin doped indium oxide (ITO) layer and a polymer layer.[10a] WO_3 also has applications in gas sensing, photocatalysis and photochromism.[11] Films containing WO_3 have been deposited by evaporation, sputtering, electrochemical techniques and by CVD.[12] WO_3 undergoes a number of phase transitions during annealing and cooling:[11] monoclinic II (< -43 ^oC) → triclinic (-43 – 17 ^oC) → monoclinic I (17 – 330 ^oC) → orthorhombic (330-740 ^oC) → tetragonal (> 740 ^oC). The monoclinic I (hereon referred to as 'monoclinic') is the most stable phase at room temperature and usually remains so even after annealing.

CVD has increasingly become the preferred method for producing metal oxide films mainly because of the higher deposition rates,[13] uniform coverage, good reproducibility, and highly dense and pure films.[14] Aerosol-assisted CVD is a variant that has additional advantages over conventional CVD which includes that the precursors do not have to be highly volatile or thermally stable.[15] This opens up the possibility of using precursors that would not have been suitable for conventional CVD such as POMs.

Keggin-type POMs have been deposited *via* AACVD[6, 16] however, this paper, to our knowledge, is the first study on the deposition of binary metal oxide thin films: vanadium doped MoO_x (x = 2-3) and WO_3 using single-source precursors called

substituted Keggin-type POMs *via* AACVD. All POMs and films were characterized spectroscopically.

Experimental

The reagents were purchased from Sigma Aldrich (99.9% purity unless stated otherwise) and used without further refinement. The identity of the POMs was confirmed by ^{31}P NMR and FT-IR which were consistent with XPS and EDX. POMs (**1- 4**) were prepared by literature procedures.[3, 17]

*Preparation of $H_4[PMo_{11}VO_{40}]$ **(1)***

POM (**1**) was synthesised following a method given by ACAL Energy Ltd which was scaled down to suit to the quantities required in the present study.[17] V_2O_5 (0.45 g, 2.47 mmol) and MoO_3 (7.92 g, 55.02 mmol) were suspended in distilled water (50 mL) with moderate stirring. 85% H_3PO_4 (0.57 g, 5.82 mmol) was added to the mixture followed by additional distilled water (45 mL). The pale yellow mixture was heated at reflux (120 ^oC). After two days, a drop of H_2O_2 was added and the mixture was left at reflux for a further five days, resulting in a clear orange/red solution. The solution was cooled to room temperature and clarified by vacuum filtration producing an orange solution. The solvent evaporated overnight in a fume hood leaving behind an orange solid.

*Preparation of $H_7[PMo_8V_4O_{40}]$ **(2)***

POM (**2**) was supplied in aqueous solution which was evaporated in a fume hood to leave behind an orange solid.[17]

Preparation of $[^nBu_4N]_4[PVW_{11}O_{40}]$ (3) and $[^nBu_4N]_5[PV_2W_{10}O_{40}]$ (4)[3]

A stock solution of V(V) was prepared by dissolving NH_4VO_3 (5.85 g, 50.01 mmol) and NaOH (4.00 g, 100 mmol) in distilled water (100 mL). $NaH_2PO_4.2H_2O$ (0.08 g, 1.43 mmol) was added to a solution of $Na_2WO_4.2H_2O$ (1.65 g, 6.32 mmol) in distilled water (80 mL) followed by the addition of conc. HCl (4.34 mL) and stirred. After stirring, the stock solution (1 mL) was added to the solution (4 mL was added when $[^nBu_4N]_5[PV_2W_{10}O_{40}]$ was prepared). The solution turned from clear to yellow or orange, respectively. Further distilled water (20 mL) was added to the solution and heated under reflux (120 ^oC) for three days. *n*-Bu_4NBr was added to the solution and the precipitates were filtered off and washed with distilled water and ethanol.

[^{n}Bu$_4$N]$_4$[PVW$_{11}$O$_{40}$] and [^{n}Bu$_4$N]$_5$[PV$_2$W$_{10}$O$_{40}$] were collected as pale yellow and yellow solids, respectively.

AACVD Procedure

The depositions were carried out in an in-house built CVD rig at 550 ^{o}C.[18] The glass substrate consisted of 50 nm SiO_2 barrier coated float-glass of size 90 × 45 × 4 mm (Pilkington NSG Ltd). The coating prevents the ions from within the glass diffusing to the surface preventing contamination of the film with metals such as sodium and calcium. The glass substrate was first cleaned with detergent and water, followed by propan-2-ol, propanone, and then air dried. The Mo films were deposited from a methanol based precursor solution ([H_4[$PMo_{11}VO_{40}$] (**1**) (7.5 x 10^{-3} M) and [H_7[$PMo_8V_4O_{40}$] (**2**) (7.5 x 10^{-3} M)) and W films used acetonitrile as the solvent ([nBu_4N]$_4$[$PVW_{11}O_{40}$] (**3**) (2.7 x 10^{-3} M) and [nBu_4N]$_5$[PV2$W_{10}O_{40}$] (**4**) (1.7 x 10^{-3} M)). Deposition time for the methanol solution and acetronitrile solutions were 30 and 45 minutes respectively. Different solvent systems were used as AACVD requires the precursor to be soluble in the solvent. Although all the POMs have a substituted keggin structure, the bulkier counter ion of the W POMs requires a less polar solvent to be soluble. The precursor solution was kept at room temperature. The aerosol of the precursor solution was generated by emersing the bubbler into a Vicks ultrasonic humidifier (at room temperature). The ultrasonic vibrations travel through the water and the flask to create the precursor aerosol mist. Nitrogen gas (99.9%; supplied by BOC) at a rate of 0.5 L/min was used to push the aerosol into the CVD chamber. Films were annealed at 600 ^{o}C in air for 30 minutes.

Analysis of the POM precursors

^{31}P NMR was performed on a Bruker AMX300 (Mo POMs) and Bruker AV400 (W POMs) at 121.4 and 162.0 MHz, respectively. The probe temperature was thermostated at 300 K and 292.4 K, respectively. The Mo POMs (**1**) and (**2**) were in a D_2O solvent system and the W POMs (**3**) and (**4**) were dissolved in CD_3CN. FT-IR analysis was carried out using a Bruker alpha platinum-ATR. Energy dispersive X-ray analysis (EDX) was carried out using a JEOL JSM-6301F Field Emission instrument with an acceleration voltage of 20 kV. Samples were placed onto conductive carbon tape that was attached to stainless steel holders. The samples were

then coated with a fine layer of carbon to stop charging. X-ray photoelectron spectroscopy (XPS) was carried out using a Thermo Scientific K-Alpha instrument with monochromatic Al-K_α source to identify the oxidation state and chemical constituents. The peaks modelled using CasaXPS software with binding energies adjusted to carbon (284.5 eV) in order to compensate for the effects of charging.

Analysis of the films

EDX and XPS analysis were performed using the same instruments as above. Scanning electron microscopy (SEM) was carried out using a JEOL JSM-6301F Field Emission instrument with acceleration voltage of 5 kV. For EDX and SEM measurements sample preparation involved cutting the films down to coupons of 10 mm x 10 mm or less and attaching them on stainless steel holders using conductive carbon tape. Contacts from the top of the film to the carbon tape were made using a solution of silver paint. The samples were then coated with a fine layer of carbon or gold, respectively, to stop charging. X-ray diffraction (XRD) was done using a microfocus Bruker D8 GAADS powder X-ray diffractometer with monochromated Cu $K_{\alpha1}$ (1.54056 Å) and Cu $K_{\alpha2}$ (1.54439 Å) radiation with an intensity ratio of 2:1, a voltage of 40 kV and current of 40 mA. The X-ray incident angle was 5^o and the detector angle was 22^o. The sample height was adjusted to focus the X-ray beam. Peak positions were compared to patterns from the Inorganic Crystal Structure Database (ICDS). The lattice parameters were calculated from powder X-ray diffraction data using the software GSAS and EXPGUI *via* the Le Bail method. UV/Vis/Near IR transmittance and reflectance spectra were produced using the Perkin Elmer Precisely Lambda 950 spectrometer using an air background and recorded between 320-2500 nm. The data obtained from this was used to calculate the band gap *via* a Tauc plot**.** Water droplet (5 µL) contact angles were carried out using an FTA-1000 drop shape instrument.

Results and discussion

Single source polyoxometalate precursors were synthesised for use in AACVD to deposit V-doped Mo and W oxide thin films. In general POM $H_4[PMo_{11}VO_{40}]$ (**1**) was synthesised *via* a reflux of V_2O_5 and MoO_3 in the presence of Na_2CO_3 and a drop of H_2O_2. POMs $[^nBu_4N]_4[PVW_{11}O_{40}]$ (**3**) and $[^nBu_4N]_5[PV_2W_{10}O_{40}]$ (**4**) were synthesised by refluxing together a solution consisting of $NaH_2PO_4.2H_2O$, $Na_2WO_4.2H_2O$, concentrated HCl, and a stock solution made of NH_4VO_3 and NaOH. These POMs, like others reported in the literature, are easy to synthesise resulting in a good yield.

The FTIR spectra of the POMs (**1**, **2**, **3** and **4**) show the characteristic bands for the Keggin structure: 780-800, 860-880 cm^{-1} (M-O-M; bridging), 960-990 cm^{-1} (M=O; terminal) and 1060-1080 cm^{-1} (P-O) where M corresponds to Mo or W.[19] However for POMs (**1**) and (**2**) these bands appear at reduced wavenumbers which is likely a feature of the substituted Keggin structure. The FTIR spectra of the W POMs (**3**) and (**4**) show an additional peak at ~1480 cm^{-1} most likely due to a C-N or a C-H stretch originating from the counter ion. It is noteworthy that bands were also seen in the 3600, 3300 and 1600 cm^{-1} region for all of the POMs, which correspond to the symmetric stretching, asymmetric stretching and bending vibrations in water, respectively.[20]

P ^{31}NMR was also carried out on the powders. The ^{31}P NMR spectra of (**1**) had a single major peak with a chemical shift of -3.0 ppm but the spectra of (**2**) contained a number of peaks including one in the region of -3 ppm. Other studies have also found multiple peaks in the NMR spectra when more than one V atom is present which is the case for (**2**).[21] The additional peaks represent different resonances due to the presence of different isomers.[21a] It has been reported in the literature that the peaks in the ^{31}P NMR for $[PV_xM_{12-x}O_{40}]$ POMs depended on the value of x.[21b] POM (**3**) containing a single vanadium atom also produced a single peak in the ^{31}P NMR spectra at -15.1 ppm[21b] and the spectra of (**4**) which has two V atoms showed a peak at -15.1 ppm and -14.1 ppm. Again, the presence of a second peak may also be explained by the different V-P resonances that arise because of the presence of different isomers.

X-ray photoelectron spectroscopy (XPS) was carried out on the four POM powders to determine their oxidation state. Sample XPS spectra for the Mo 3d and W 4f transitions of POM (**1**) and (**3**) is shown in Figure 1. The Mo based POMs (**1**) and (**2**) showed Mo $3d_{5/2}$ peaks at 232.9 and 232.7 eV respectively corresponding to Mo in the +6 oxidation state.[6, 22] Peaks at lower binding energies corresponding to reduced states in the Mo 3d XPS spectra were also observed. This is common occurrence for Mo^{6+} species during XPS analysis.[23] XPS of POMs (**3**) and (**4**) showed W in the +6 oxidation state with both W 4f7/2 binding energies at 35.3 eV. [16, 24] All four POMs contained P and V in the +5 oxidation state as indicated by binding energies of 133.5 (±0.2) and 517 (±0.5) eV respectively.[25] [26]

The binding energy range for the O was between 530.5-533.6 eV matching ranges found in literature.[6, 27] There are four O environments in the substituted Keggin POMs in comparison with the three for a standard Keggin POM structure (the extra M-O environment; where M = Vanadium).

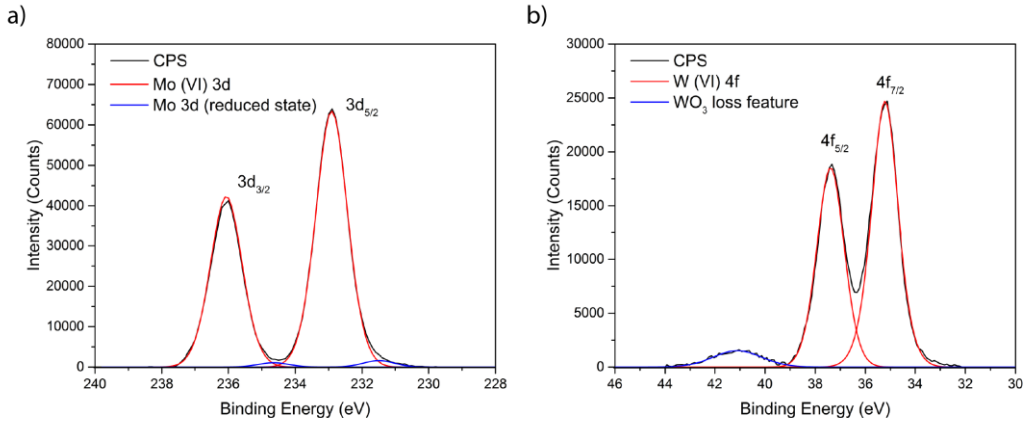

Figure 1: Example XPS spectra of the Mo 3d and W 4f transitions for POM (1) and (3) respectively. The Mo 3d5/2 peak in POM appears at 232.9 eV corresponding to Mo^{6+} and the W 4f7/2 peak is centred at 35.3 eV matching W^{6+}.

Energy dispersive X-ray spectroscopy (EDX) was used to determine atomic ratios of the POM powders (Table 1). The POMs are in close agreement with the stated formula of the anions. The discrepancies could be explained by the presence of other POMs that may have been synthesised, such as $[PMo_{12}O_{40}]^{n-}$, since the methods of synthesis are similar.

Table 1: The approximate ratio of atoms relative vanadium in the POMs. An average of the atomic ratios was by analysis three different areas per sample.

POM	Approximate ratio of atoms relative to vanadium			
	P	Mo/W	V	O
$H_4[PMo_{11}VO_{40}]$ (**1**)	1	12	1	37
$H_7[PMo_8V_4O_{40}]$ (**2**)	1	9	4	38
$[^nBu_4N]_4[PVW_{11}O_{40}]$ (**3**)	2	10	1	42
$[^nBu_4N]_5[PV_2W_{10}O_{40}]$ (**4**)	2	11	2	49

The POM powders - $H_4[PMo_{11}VO_{40}]$ (**1**), $H_7[PMo_8V_4O_{40}]$ (**2**), $[^nBu_4N]_4[PVW_{11}O_{40}]$ (**3**) and $[^nBu_4N]_5[PV_2W_{10}O_{40}]$ (**4**) – were then used as precursors in the deposition of V doped α-MoO_3 and WO_3 thin films. AACVD was carried out at 550 ^oC using nitrogen as a carrier gas at a flow rate of 0.5 L/min. Methanol and acetonitrile were used as the solvents in the deposition of Mo and W films respectively.

V doped α-MoO_3 from $H_4[PMo_{11}VO_{40}]$ (**1**) and $H_7[PMo_8V_4O_{40}]$ (**2**)

Methanol solutions of $H_4[PMo_{11}VO_{40}]$ (**1**) and $H_7[PMo_8V_4O_{40}]$ (**2**) were used as precursors to deposit V-doped α-MoO_3 thin films. The as deposited black, non-adherant and X-ray amorphous films were annealed under air at 600 ^oC for 30 minutes. The annealed films were translucent yellow in appearance and well adhered to the substrate, passing the Scotch^{TM} tape test.

X-ray diffraction studies showed that the annealed films were crystalline and consisted of orthorhombic α-MoO_3 with preferential orientation (Figure 2).

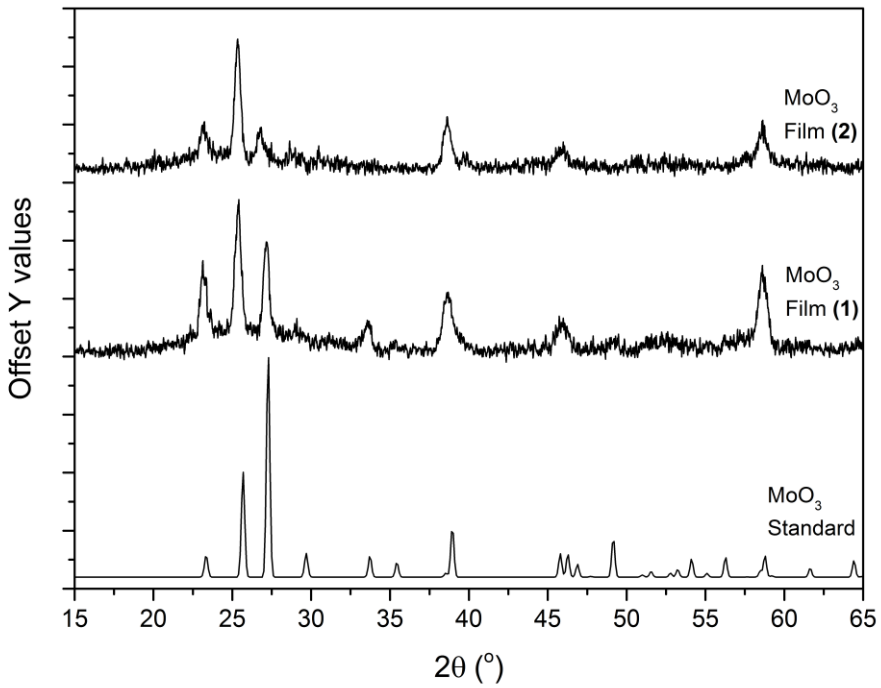

Figure 2: XRD pattern of the films deposited from POMs, $H_4[PMo_{11}VO_{40}]$ (1) and $H_7[PMo_8V_4O_{40}]$ (2).

The diffraction patterns of films (**1**) and (**2**) were fitted to a Le Bail refined model which an approximately 4% expansion in the α-MoO_3 unit cell compared to standard values (Table 2) - this is consistent with the observed shift to lower 2θ values in the XRD patterns.[28] The expansion also suggested that substitutional doping of α-MoO_3 with V^{5+} had not occurred as the ionic radii of V^{5+} is smaller than that of Mo^{6+}. However, due to the layered nature α-MoO_3 it is possible that V^{5+} is intercalated leading to the observed expansion in the unit cell of the α-MoO_3. This has previously been reported with Li ions forming Li_xMoO_3 precipitates between layers of MoO_3.[29]

Table 2: Lattice parameters of films from POMs $H_4[PMo_{11}VO_{40}]$ (1) and $H_7[PMo_8V_4O_{40}]$ (2) calculated from XRD data *via* the Le Bail method.

Film	a / Å	b / Å	c / Å	Unit Cell Volume / Å	Volume expansion / %
$H_4[PMo_{11}VO_{40}]$ (**1**)	4.0135(7)	14.308(4)	3.6772(4)	211.16(8)	4.05(9)
$H_7[PMo_8V_4O_{40}]$ (**2**)	3.996(1)	14.044(4)	3.759(3)	211.0(2)	3.99(3)

Furthermore, the 4% expansion in the α-MoO_3 framework of both films is in spite of film (**2**) having a higher V content compared to film (**1**) as determined by EDX analysis. This suggests that the excess V in film (**2**) may exists in the amorphous oxide form.

Mo in the annealed films (**1**) and (**2**) was in the +6 oxidation state as shown by a 3d5/2 peaks for both films at 232.7 eV (Figure 3a). As with the XPS spectra of the POM powders, peaks at lower binding energies (230.9 eV) corresponding to reduced surface states were observed.[23] XPS also showed the dopant V species to be in the +5 oxidation state with 2p3/2 peaks for the two α-MoO_3 films centered at 517.1 eV (Figure 3b).[30]

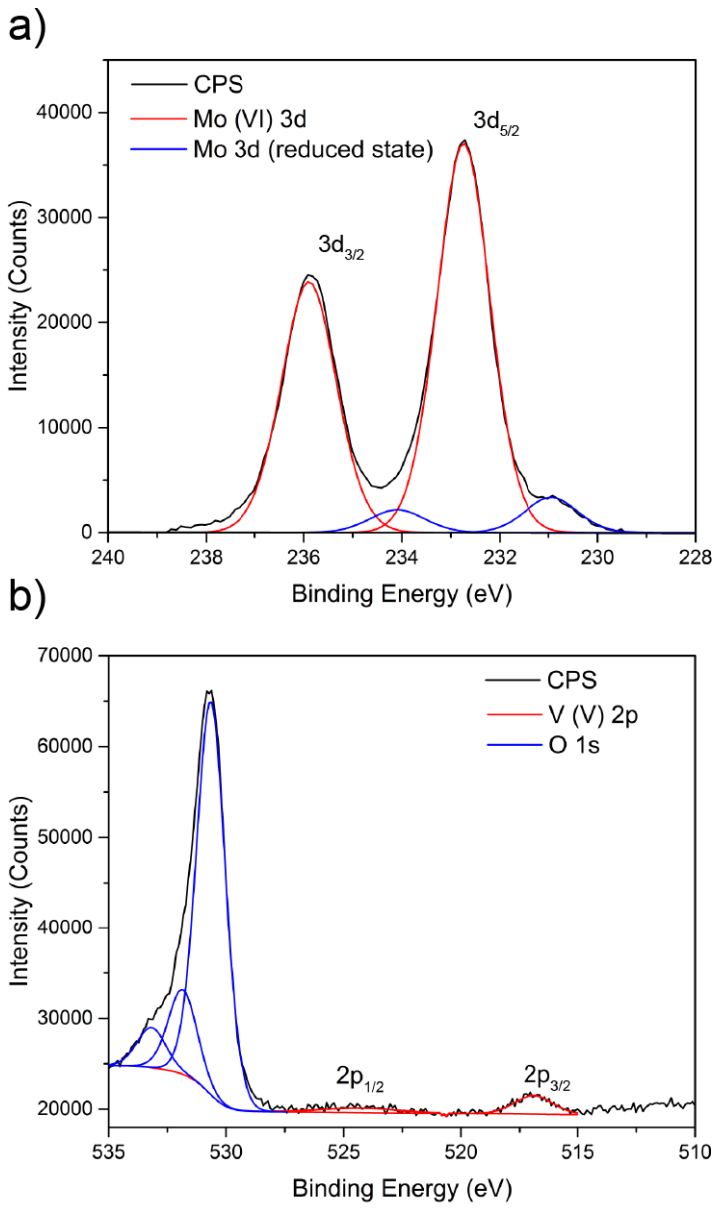

Figure 3: a) Sample XPS spectrum of Mo 3d taken from α-MoO_3 film 1. The 3d5/2 peak was seen at 232.7 eV corresponding to Mo^{3+}, a peak at 230.9 eV corresponds to 3d5/2 peak for Mo in a reduced state. b) Sample XPS spectrum of the V 3d and O 1s peaks. V2p3/2 at 517.1 eV matches well with literature reports for V^{5+}.

Figure 4 shows the surface morphology of the α-MoO_3 films as probed with a scanning electron microscope. Film (**1**) was dominated by clusters of irregularly stacked diamond shaped flat discs. The diamond shaped discs were almost regular in shape (0.5 x 0.3 μm) with a thickness of 0.1 μm. Film (**2**) consisted of a mixture of tapered long needles and spherical particles. The long needles appeared to be roughly the same size (1.5 x 0.2 μm) and the majority of the spherical particles had a diameter of 0.5-2 μm. In both films the space between the particles is assumed to be bare glass.

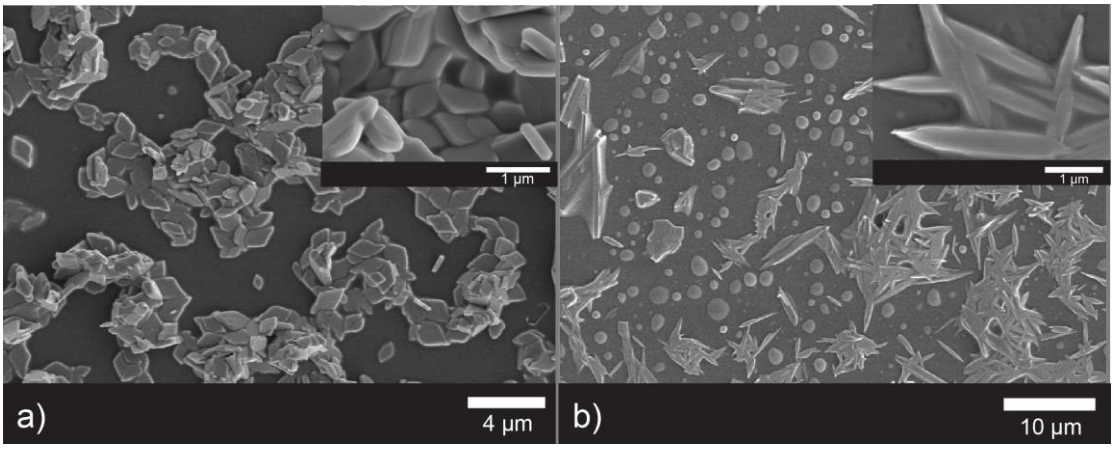

Figure 4: SEM of films produced using POMs $H_4[PMo_{11}VO_{40}]$ (1) and $H_7[PMo_8V_4O_{40}]$ (2).

As expected films (**1**) and (**2**) showed high transmittance with the latter having a much greater transparency of ~90% at 550 nm (Figure 5). The observed variation between the two films is most likely an outcome of the composition of the POM used for depositing the MoO_3 films.

The indirect band gaps were calculated using data collected from UV-vis *via* the Tauc plot.[31] The band gaps for the V-doped MoO_3 films (**1**) and (**2**) were 2.85 eV and 2.98 eV, respectively. The band gaps of these are in close agreement with literature values for the polycrystalline structure (2.8 eV).[23]

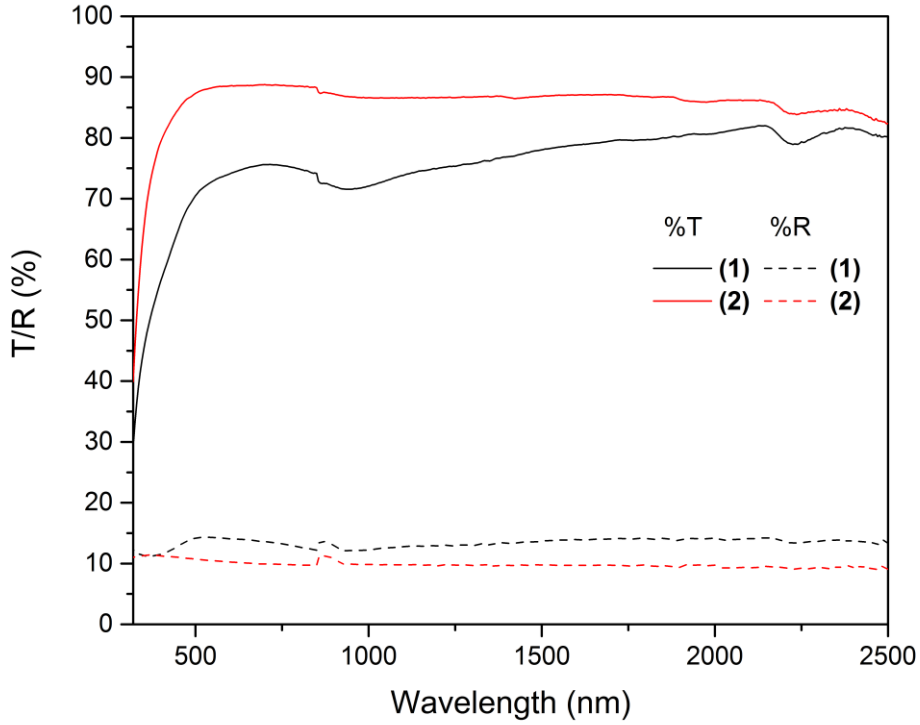

Figure 5: The transmission (black) and reflectance (red) spectra for the films using the POMs $H_4[PMo_{11}VO_{40}]$ (1) (solid line) and $H_7[PMo_8V_4O_{40}]$ (2) (dashed line).

V doped WO_3 from $[^nBu_4N]_4[PVW_{11}O_{40}]$ (**3**) and $[^nBu_4N]_5[PV_2W_{10}O_{40}]$ (**4**)

The W POMs - $[^nBu_4N]_4[PVW_{11}O_{40}]$ (**3**) and $[^nBu_4N]_5[PV_2W_{10}O_{40}]$ (**4**) - were used as precursors to deposit V doped WO_3 in an acetonitrile solution at 550 ^oC and a nitrogen flow rate of 0.5 L/min. Brown poorly adherent films were deposited on the top plate and XRD showed that they were amorphous. Upon annealing at 600 ^oC for 30 minutes the films became adherent and translucent. XRD showed that the annealed films were crystalline monoclinic WO_3 (Fig. 5). The annealed films were studied using a variety of analytical techniques.

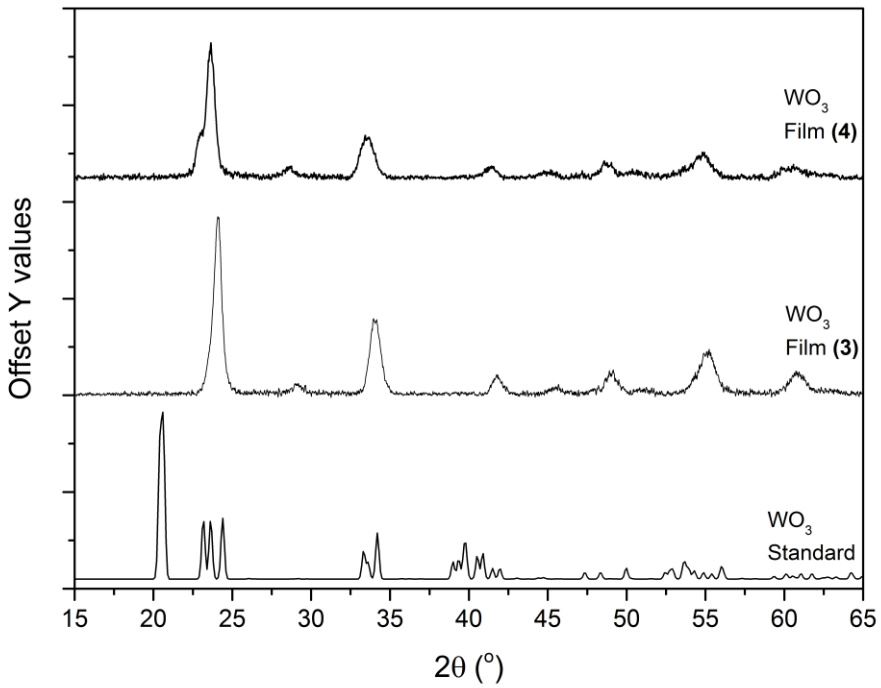

Figure 6: The XRD pattern of the tungsten films deposited using the POMs [^{n}Bu$_4$N]$_4$[PVW$_{11}$O$_{40}$] (3) and [^{n}Bu$_4$N]$_5$[PV$_2$W$_{10}$O$_{40}$] (4).

A minor shift in the XRD pattern was observed when compared to a standard WO_3 pattern.[32] Films from (**3**) and (**4**) were fitted to a Le Bail refined model which indicated that the unit cell of (**3**) shows a minor contraction of 0.23%, however this is within error hence the unit cell size volume remains similar (Table 5). The unit cell of (**4**) had expanded by ~3%, indicating possible interstitial doping of V into the WO_3 unit cell as V^{5+} has a smaller ionic and crystal radii than W^{6+} (Table 5).

Table 3: Lattice parameters of films deposited from POMs [^{n}Bu$_4$N]$_4$[PVW$_{11}$O$_{40}$] (3) and [^{n}Bu$_4$N]$_5$[PV$_2$W$_{10}$O$_{40}$] (4) calculated from XRD data *via* the Le Bail method.

Film	a / Å	b / Å	c / Å	Unit Cell Volume / Å	Volume Change / %
[^{n}Bu$_4$N]$_4$[PVW$_{11}$O$_{40}$] (**3**)	7.281(1)	7.5429(3)	7.6975(7)	422.77(7)	0.23(3)
[^{n}Bu$_4$N]$_5$[PV$_2$W$_{10}$O$_{40}$] (**4**)	7.400(1)	7.5932(9)	7.755(1)	435.72(11)	2.83(1)

XPS analysis showed the presence of W and V in the AACVD grown WO3 films (**3**) and (**4**) (Figure 7). The W 4f7/2 peak was at 35.5 eV and 35.3 eV respectively, thus confirming the presence of W^{+6}.[33] The peak for V2p3/2 appears at 517.2 eV matching to V^{+5}.[34]

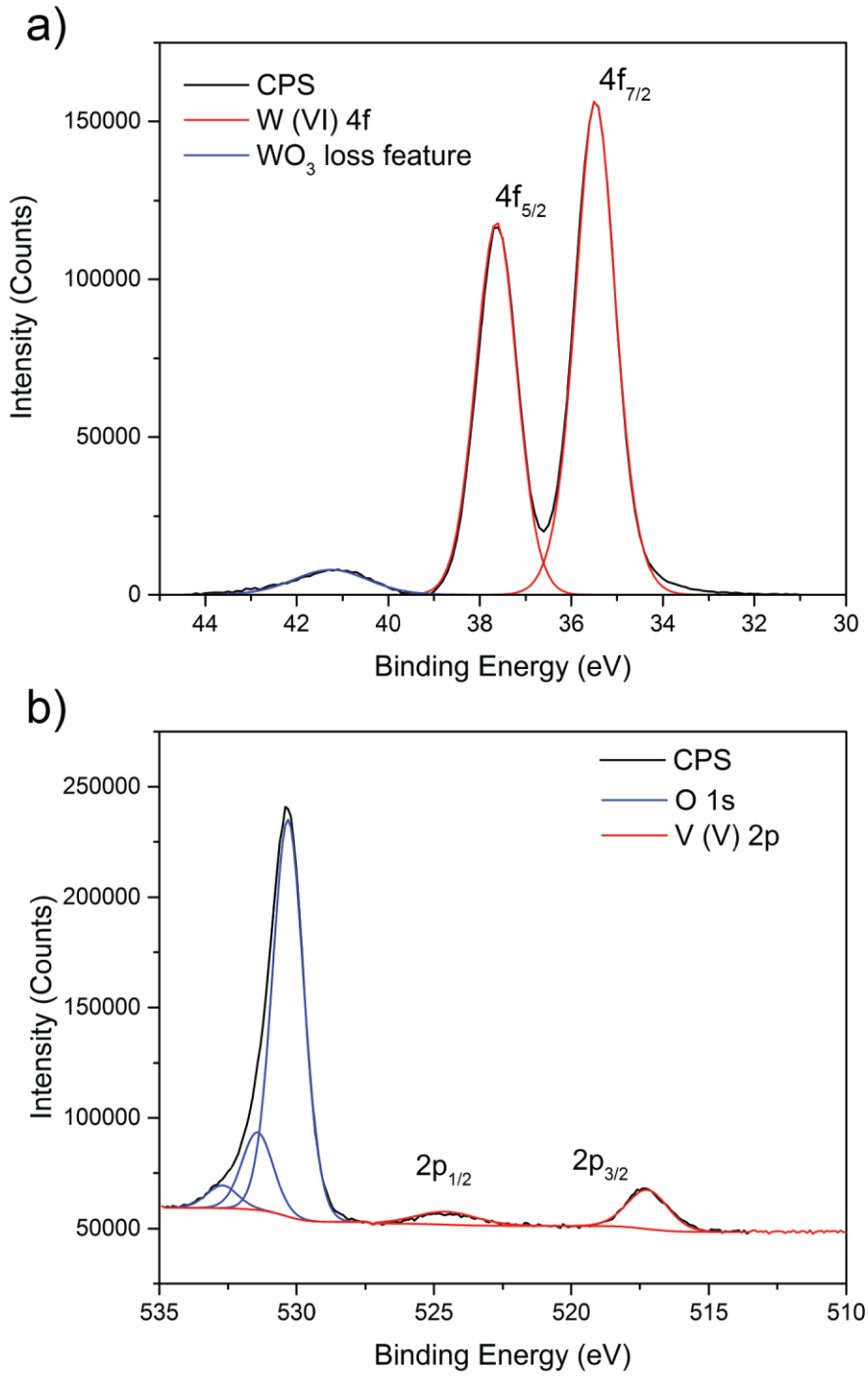

Figure 7: a) The XPS spectrum for W 4f (film (3)) showing the $4f_{7/2}$ peak positioned at 35.5 eV - matching W^{+6}. b) The V in films from (3) and (4) was in the +5 oxidation state as evident from the V 2p3/2 peak being centered at 517.2 eV.

The morphology of films (**3**) and (**4**) is shown in Figure 8. Film (**3**) consists of a porous network of particles that are 250 nm or smaller which cover the whole area analysed. Film (**4**) is however composed of clusters of WO_3 which are made up of

particles that up to 250 nm in width. Both films have varying morphologies even though they consist of WO_3 which, as with films (**1**) and (**2**), is due to the nature of the POM used to deposit the films.

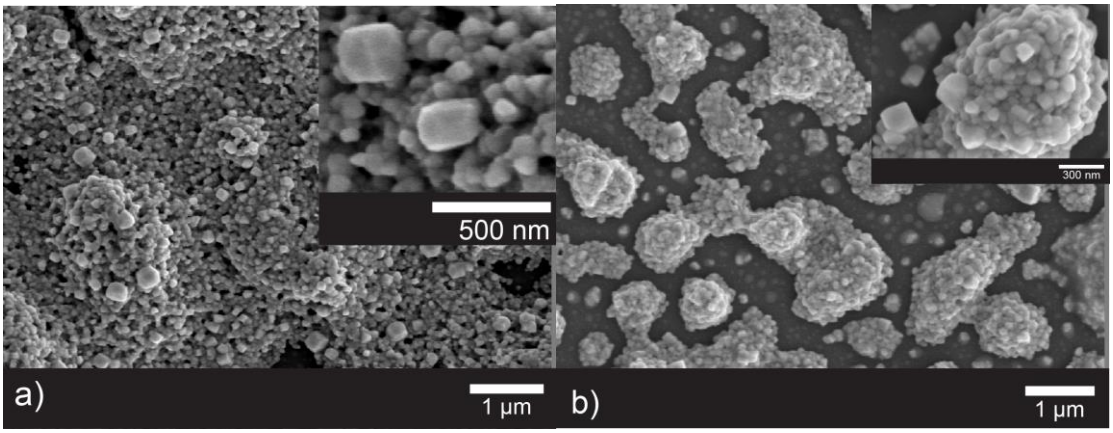

Figure 8: SEM of the tungsten films, deposited using the POMs, $[^{n}Bu_4N]_4[PVW_{11}O_{40}]$ (3) and $[^{n}Bu_4N]_5[PV_2W_{10}O_{40}]$ (4).

The maximum transmittance at 550 nm was observed to be ~85% for the film deposited from POM (**4**) whereas film (**3**) reached similar maxima but at a higher wavelength (Fig. 7). In general, all films were found be poorly reflective (<18%).

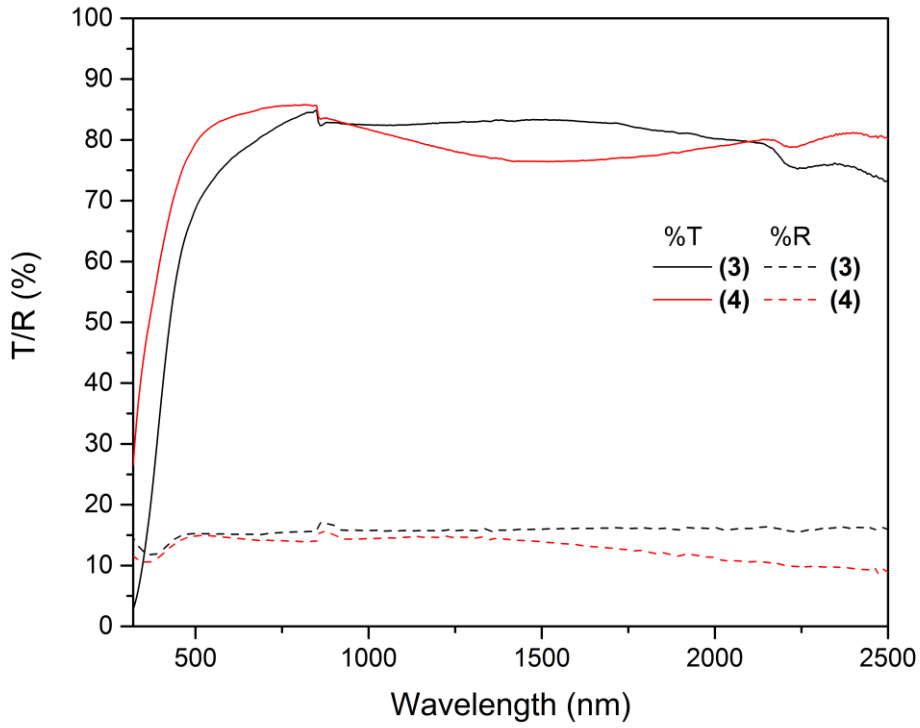

Figure 9: The transmission (black) and reflectance (Red) spectra of the tungsten films deposited using the POMs, $[^{n}Bu_4N]_4[PVW_{11}O_{40}]$ (3) (solid line) and $[^{n}Bu_4N]_5[PV_2W_{10}O_{40}]$ (4) (dashed line).

The band gaps of these films were calculated using the same method described for films **1** and **2** (see above)**.** The band gaps were found to be 2.6 eV and 2.7 eV for films from POMs (**3**) and (**4**), respectively, lower than the value (3.2 eV) for un-doped tungsten oxide films.[35] Although doping generally increases the band gap due to the Moss-Burstein effect,[18] there have been reports suggesting that doping vanadium into WO_3 can reduce the bandgap.[4a]

Water contact angles

Water contact angles were calculated for the films. Film from POM (**1**) had a water contact angle of 98.5^{o} indicative of a hydrophobic nature whereas (**2**) had an angle of 41.6^{o} suggesting it is hydrophilic. The films differed in V atom content and morphology. Therefore, it would seem reasonable to suggest that the hydrophobicity of the film was reduced with greater V doping and/or film morphology (Fig. 3). Ashraf *et al*.[6] found MoO_2 films to have a water contact angle between 75-125^{o} and a needle-like morphology. However, in the present study, it was the film from (**2**) that had a needle-like morphology (Fig. 3). The water contact angles for the W films (**3**) and (**4**) were much lower, with angles of 22.7^{o} and 13.4^{o}, respectively, suggesting that the films were hydrophilic in nature. These are in good agreement with literature values for WO_3 films annealed at 500 ^{o}C.[36]

Conclusion

The present study has showed the use of polyoxometalates, with general formula $[PM_{12-x}V_xO_{40}]^{n-}$ (M=Mo or W), as single-source precursors to form vanadium doped metal-oxide films *via* aerosol assisted chemical vapour deposition. This technique was an advantageous method as the precursor only needed to be soluble in a suitable solvent and volatility was not a requirement. Depositions were carried out at 550 ^{o}C with methanol or acetonitrile as the solvent for Mo and W, respectively. The POMs (**1**) and (**2**) deposited films were amorphous and non-adherent. However, on annealing the films consisted of vanadium-doped MoO_3. The films deposited using the tungsten POMs, (**3**) and (**4**), also followed a similar trend with the as-deposited films being amorphous and after annealing they were characterised as vanadium-doped WO_3. The

range of film morphologies obtained had important implications on the water contact angles of the film.

It can be concluded that POMs provide a single-source route to the formation of doped metal oxide films; furthermore controlled amounts of dopants could be incorporated, to some extent, into the film, which have implications on the functional properties.

Acknowledgements

EPSRC are thanked for a studentship (SDP) and for grant no. EP/K001515. NSG are thanked for the glass substrates. Kevin Reeves and Abil Aliev are thanked for their assistance in SEM and NMR, respectively.

References

[1] X. Lopez, J. J. Carbo, C. Bo, J. M. Poblet, *Chemical Society Reviews* **2012**, *41*, 7537-7571.

[2] aY.-F. Song, R. Tsunashima, *Chemical Society Reviews* **2012**, *41*, 7384-7402; bK. C. Dey, V. Sharma, *International Journal of ChemTech Research* **2010**, *2*, 368-375; cW. Yang, L.-H. Gao, K.-Z. Wang, *Polyhedron* **2014**, *82*, 80-87.

[3] T. Ueda, M. Komatsu, M. Hojo, *Inorganica Chimica Acta* **2003**, *344*, 77-84.

[4] aC.-W. Yeh, C.-H. Hung, K.-R. Wu, C.-C. Yang, *Environmental Engineering Science* **2014**, *31*, 42-48; bA. Kubacka, G. Colón, M. Fernández-García, *Catalysis Today* **2009**, *143*, 286-292; cZ. Wenfang, L. Qingju, Z. Zhongqi, Z. Ji, *Journal of Physics D: Applied Physics* **2010**, *43*, 035301.

[5] T. Ivanova, K. A. Gesheva, G. Popkirov, M. Ganchev, E. Tzvetkova, *Materials Science and Engineering: B* **2005**, *119*, 232-239.

[6] S. Ashraf, C. S. Blackman, G. Hyett, I. P. Parkin, *Journal of Materials Chemistry* **2006**, *16*, 3575-3582.

[7] H. Hu, I. E. Wachs, *The Journal of Physical Chemistry* **1995**, *99*, 10911-10922.

[8] C. Zollfrank, K. Gutbrod, P. Wechsler, J. P. Guggenbichler, *Materials Science and Engineering: C* **2012**, *32*, 47-54.

[9] J. Meyer, S. Hamwi, M. Kröger, W. Kowalsky, T. Riedl, A. Kahn, *Advanced Materials* **2012**, *24*, 5408-5427.

[10] aM. Vasilopoulou, G. Papadimitropoulos, L. C. Palilis, D. G. Georgiadou, P. Argitis, S. Kennou, I. Kostis, N. Vourdas, N. A. Stathopoulos, D. Davazoglou, *Organic Electronics* **2012**, *13*, 796-806; bS. Han, W. S. Shin, M. Seo, D. Gupta, S.-J. Moon, S. Yoo, *Organic Electronics* **2009**, *10*, 791-797.

[11] H. Zheng, J. Z. Ou, M. S. Strano, R. B. Kaner, A. Mitchell, K. Kalantar-zadeh, *Advanced Functional Materials* **2011**, *21*, 2175-2196.

[12] D. Gogova, K. Gesheva, A. Szekeres, M. Sendova-Vassileva, *physica status solidi (a)* **1999**, *176*, 969-984.

[13] T. Ivanova, A. Szekeres, M. Gartner, D. Gogova, K. A. Gesheva, *Electrochimica Acta* **2001**, *46*, 2215-2219.

[14] K. L. Choy, *Progress in Materials Science* **2003**, *48*, 57-170.

[15] aP. Marchand, I. A. Hassan, I. P. Parkin, C. J. Carmalt, *Dalton Transactions* **2013**, *42*, 9406-9422; bC. E. Knapp, C. J. Carmalt, *Chem. Soc. Rev.* **2016**; cS. Sathasivam, R. R. Arnepalli, K. K. Singh, R. J. Visser, C. S. Blackman, C. J. Carmalt, *RSC Advances* **2015**, *5*, 11812-11817; dS. Sathasivam, R. R. Arnepalli, B. Kumar, K. K. Singh, R. J. Visser, C. S. Blackman, C. J. Carmalt, *Chem. Mater.* **2014**, *26*, 4419-4424; eS. Ponja, S. Sathasivam, N. Chadwick, A. Kafizas, S. M. Bawaked, A. Y. Obaid, S. Al-Thabaiti, S. N. Basahel, I. P. Parkin, C. J. Carmalt, *J. Mater. Chem. A* **2013**, *1*, 6271-6278; fS. Sathasivam, D. S. Bhachu, Y. Lu, N. Chadwick, S. A. Althabaiti, A. O. Alyoubi, S. N. Basahel, C. J. Carmalt, I. P. Parkin, *Scientific reports* **2015**, *5*.

[16] S. Ashraf, C. S. Blackman, R. G. Palgrave, I. P. Parkin, *Journal of Materials Chemistry* **2007**, *17*, 1063-1070.

[17] J. H. Grate, D. R. Hamm, R. J. Saxton, M. T. Muraoka, Catalytica, Inc., Mountain View, California, United States, **1996**, p. 36.

[18] S. D. Ponja, S. Sathasivam, I. P. Parkin, C. J. Carmalt, *RSC Advances* **2014**, *4*, 49723-49728.

[19] H. Benaissa, P. N. Davey, Y. Z. Khimyak, I. V. Kozhevnikov, *Journal of Catalysis* **2008**, *253*, 244-252.

[20] B. M. Auer, J. L. Skinner, *The Journal of Chemical Physics* **2008**, *128*, 224511.

[21] aL. Pettersson, I. Andersson, J. H. Grate, A. Selling, *Inorganic Chemistry* **1994**, *33*, 982-993; bM. A. Fedotov, R. I. Maksimovskaya, *J Struct Chem* **2006**, *47*, 952-978.
[22] J.-H. Bihn, J.-Y. Park, Y.-C. Kang, *Journal of the Korean Physical Society* **2011**, *58*, 509-514.
[23] D. O. Scanlon, G. W. Watson, D. J. Payne, G. R. Atkinson, R. G. Egdell, D. S. L. Law, *The Journal of Physical Chemistry C* **2010**, *114*, 4636-4645.
[24] X. P. Wang, B. Q. Yang, H. X. Zhang, P. X. Feng, *Nanoscale Res Lett* **2007**, *2*, 405-409.
[25] P. Vassileva, V. Krastev, L. Lakov, O. Peshev, *J Mater Sci* **2004**, *39*, 3201-3202.
[26] aE. Hryha, E. Rutqvist, L. Nyborg, *Surface and Interface Analysis* **2012**, *44*, 1022-1025; bQ.-H. Wu, A. Thissen, W. Jaegermann, M. Liu, *Applied Surface Science* **2004**, *236*, 473-478.
[27] M. E. A. Warwick, C. W. Dunnill, R. Binions, *Chemical Vapor Deposition* **2010**, *16*, 220-224.
[28] T. Leisegang, A. A. Levin, J. Walter, D. C. Meyer, *Crystal Research and Technology* **2005**, *40*, 95-105.
[29] J. W. Bullard Iii, R. L. Smith, *Solid State Ionics* **2003**, *160*, 335-349.
[30] W. E. Slink, P. B. DeGroot, *J. Catal.* **1981**, *68*, 423-432.
[31] J. Tauc, *Materials Research Bulletin* **1968**, *3*, 37-46.
[32] T. Vogt, P. M. Woodward, B. A. Hunter, *Journal of Solid State Chemistry* **1999**, *144*, 209-215.
[33] F. Y. Xie, L. Gong, X. Liu, Y. T. Tao, W. H. Zhang, S. H. Chen, H. Meng, J. Chen, *Journal of Electron Spectroscopy and Related Phenomena* **2012**, *185*, 112-118.
[34] G. Silversmit, D. Depla, H. Poelman, G. B. Marin, R. De Gryse, *Journal of Electron Spectroscopy and Related Phenomena* **2004**, *135*, 167-175.
[35] K.-S. Ahn, S.-H. Lee, A. C. Dillon, C. E. Tracy, R. Pitts, *Journal of Applied Physics* **2007**, *101*, -.
[36] R. Azimirad, N. Naseri, O. Akhavan, A. Z. Moshfegh, *Journal of Physics D: Applied Physics* **2007**, *40*, 1134.